Acta Cryst. (1999). A**55**, 204–211

Divergent-beam technique used in a SEM to measure the cell parameters of isotopically distinct samples of LiF over the temperature range ~15–375 K

MONICA J. MENDELSSOHN* AND H. JUDITH MILLEDGE

Crystallography and Mineral Physics Unit, Research School of Geological and Geophysical Sciences, Birkbeck and University College London, Gower Street, London WCIE 6BT, England. E-mail: m.mendelssohn@ucl.ac.uk

(*Received 3 February 1998; accepted 27 August 1998*)

Dedicated to Professor A. F. Moodie on the occasion of his 75th birthday

Abstract

The cell parameters for LiF containing 90.4% ^{6}Li and 50.2% ^{6}Li were determined from a series of divergent-beam photographs taken at approximately 25 K intervals in the ~15 to 375 K range. The divergent-beam photographs were generated in a Stereoscan S4 scanning electron microscope fitted with a liquid-helium cold finger and a Dingley Kossel camera. Lattice parameters can be determined from the ratios of lines joining conic intersections, and such data, measured on films taken at known temperatures, were correlated with equivalent data from computer-generated divergent-beam patterns using appropriate cell parameters; our cell parameters at 298 K are $^6Li_{90.4\%} = 4.0272\ (2)$ and $^6Li_{50.2\%.} = 4.0266\ (2)$ Å. If it is assumed that the stated isotopic compositions are correct, linear extrapolation to end-member cell parameters gives $^6Li_{100\%} = 4.0273\ (2)$ and $^6Li_{0\%} = 4.0259\ (2)$ Å. Since for a cubic crystal only one lattice-parameter measurement is required from each photograph, the usefulness of the ratio approach was tested by comparing values of the lattice parameter deduced from many such ratios obtained from photographs with no symmetry and with mirror symmetry.

1. Introduction

All chemical processes depend on the nature of the potential functions between the atoms involved. Such a function has a minimum at the preferred interatomic separation of the atoms, which in turn depends on the masses of the atoms and the strength of the bonds. Increased mass leads to shorter bonds and higher melting points for the isotopes of a particular element, and thus, in principle, to different phase diagrams for different isotopes. Whereas isotopic differences have few consequences in ordinary life, the immense time scales and extremely slow rates of temperature change involved in geological processes enable diffusion and exchange phenomena, which are dependent on atomic masses, to produce measurable isotope fractionations. Deductions based on such data are still largely empirical, but a knowledge of the cell parameters of the end members of isotopic solid solutions, and hence of the atomic volumes of individual isotopes, near absolute zero would enable the behaviour of isotopically distinct systems to be modelled in relation to geological processes.

Most elements are in fact solid solutions consisting of two or more stable isotopes having the natural abundances shown diagramatically in Fig. 1. The molar volumes of these isotopes will be different at temperatures at which zero-point energy is important; for very hard materials such as diamond and cubic BN, lattice-parameter differences can be detected at room temperature and pressure (RTP), but for most elements

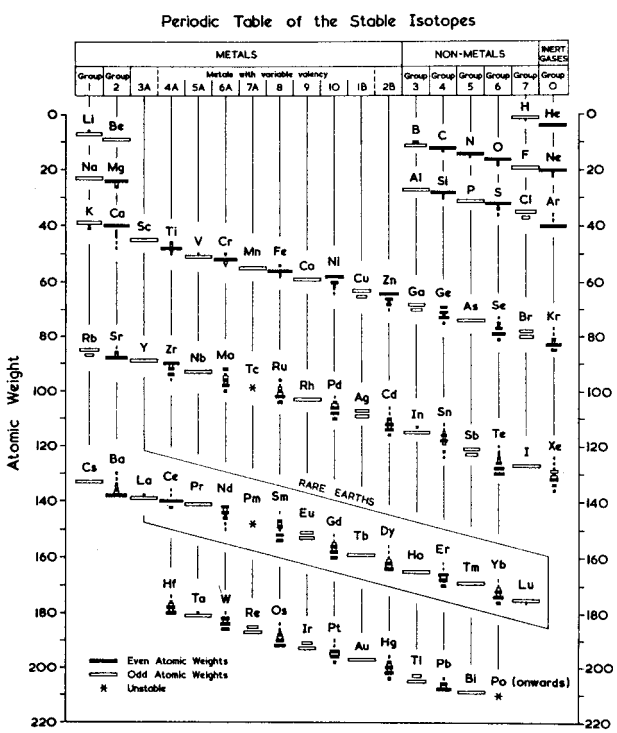

Fig. 1. Diagrammatic representation of the isotopic compositions of the stable elements.

and compounds significant differences can only be expected near absolute zero.

In order to investigate the variation in cell parameter as a function of temperature, it is desirable to select an element with only two isotopes having a large percentage mass difference and a melting point well above the temperature range available in the experimental system (here ~10–380 K). Since it is not feasible to work with pure lithium, the compound LiF was selected because it is cubic, is the type compound for the alkali halides, and the other element involved, fluorine, is mono-isotopic. As the difference in mass between the two isotopes of lithium is relatively large, significant cell-parameter differences may be expected for lithium compounds near absolute zero. Large single crystals belonging to the isotopic solid solution ^{6}LiF–^{7}LiF had been prepared for an investigation of the isotope effect on thermal conductivity (Berman & Brock, 1965), for which the results are shown in Fig. 8.1 of Berman (1976), and we are grateful to Dr R. Berman for giving us these crystals (90.4, 50.2 and 0.02% ^{6}LiF) for use in our experiments. Furthermore, room-temperature cell parameters for ^{6}LiF and ^{7}LiF have been determined by Thewlis (1955) using the Straumanis method, and thus provide a check on our results. Thewlis took particular care to obtain pure crystals, but the thermal conductivity data for Berman's crystals indicated that impurities other than ^{6}LiF must be present in the purest ^{7}LiF crystals, and this must, in principle, increase their lattice parameter slightly, since no possible contaminant atom is smaller than Li.

2. The divergent-beam method

The divergent-beam method has been described in detail by Lonsdale (1947). Fig. 2 (Fig. 1 from Lonsdale, 1947) shows a solid cone of X-radiation produced by the point source *S*; as the cone passes through the crystal any individual family of planes (*P*) will reflect back (*AR*) that section of the cone that is at the Bragg angle to the set of planes. The selective removal of this part of the solid cone results in a depletion conic (*QQ*) on the film (*FF*). The divergent-beam method has a number of advantages for making lattice-parameter measurements: (*a*) the sharpness of depletion conics depends only on the size of the point source and is independent of crystal thickness; (*b*) as $\theta \rightarrow 90^\circ$, the resolution of the α_1, α_2 and β lines provides comparative patterns; (*c*) triple points, *i.e.* positions where three conics $(h_1k_1l_1)$, $(h_2k_2l_2)$ and $(h_1+h_2, k_1+k_2, l_1+l_2)$ must intersect, exist and are defined more clearly than intersections where the two conics are far from orthogonal; (*d*) any minor missetting, which can accompany temperature changes, is unimportant.

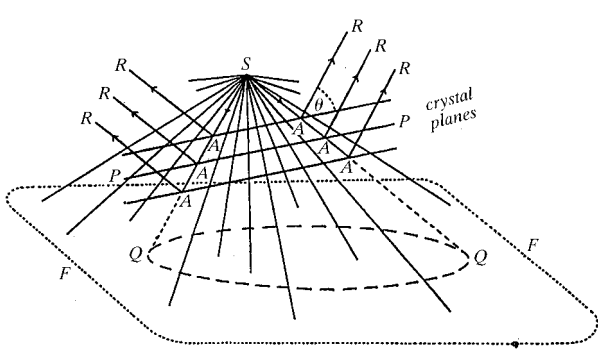

Fig. 2. The origin of deficiency conics *QQ* on X-ray diffraction photographs. Reprinted with permission from Lonsdale (1947). Copyright (1947) Royal Society.

The complete divergent-beam pattern (Figs. 3*a*, *b*) consists of a large number of intersecting conics, where the axis of each cone is parallel to the normal to a family of planes (*hkl*) and the semi-apical angle is $90 - \theta_{hkl}$. Since the positions of the conic intersections depend on

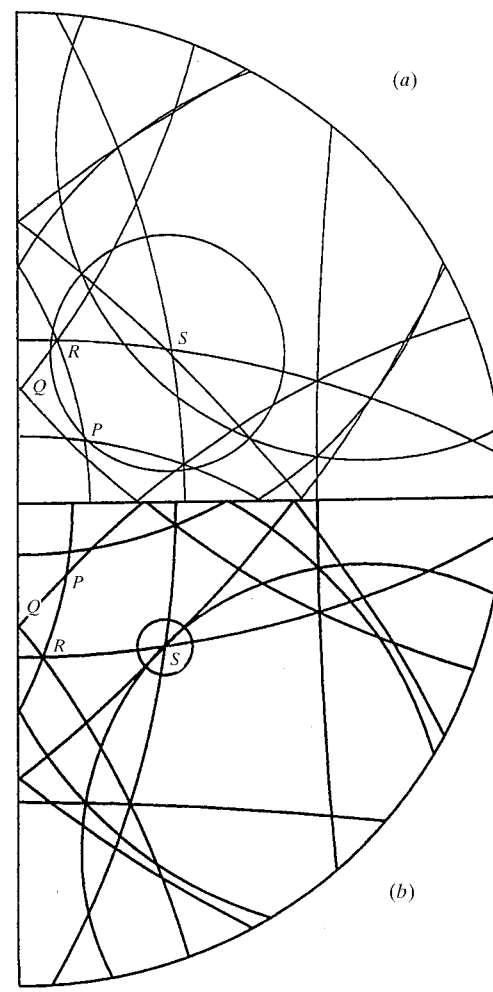

Fig. 3. Quadrants of the complete [001] divergent-beam pattern for the strongest reflections for LiF using Cu $K\alpha_1$ radiation, assuming $a = 4.05$ and $a = 4.00$ Å. If the positions of, for example, the intersections *P*, *Q*, *R* and *S* are measured, the ratios of the six lines *PQ*/*RS*, *PR*/*QS etc.* will have specific values for a given cell parameter. It can be seen that intersections that appear good at one temperature may not be so at another.

the interplanar spacings and the relative orientation of the families of planes $(hkl)_i$ and $(hkl)_j$ involved, they can be used to determine cell parameters for crystals of any symmetry from a single-crystal setting, provided that this involves the intersection of suitable conics. By varying the temperature of the crystal, a series of such photographs can be used to obtain thermal-expansion data very rapidly. In the case of cubic crystals, the relative orientations of the planes are invariant, so that only a single cell parameter has to be obtained from any one photograph. Accordingly, multiple measurements have been made from each photograph in order to establish the reproducibility of line ratio data.

The positions of the conic intersections can be measured from the films, and hence ratios of line lengths joining two intersections for known temperatures can be determined experimentally. Ratios of these line lengths for known values of the cell parameters are calculated as part of the graphical simulations. From a comparison of these two sets of ratios, the variation of the cell parameters with temperature can be evaluated and, by using the nondimensional quantity of a line length ratio, all apparatus-dependent parameters such as specimen-to-film distance are eliminated from calculations. There is, however, one experimental parameter remaining, and that is differential film shrinkage. This is known to be greater in the rolling direction of sheet film and, as the orientation of commercially available cut film is unknown, it is generally allowed for either by means of fiducial marks or, for example, Straumanis mounting. It may vary from one film to another and its importance will vary with the relative orientations of the lines being ratioed. It may account for some of the apparently random variations seen in our data, but has not been investigated.

3. Computer-aided window selection

The data extracted from the films are the coordinates of the intersections, and therefore the accuracy of the final results is dependent on the quality of the intersections, and the accuracy to which they can be measured. Factors to be considered when selecting 'good' intersections (see Fig. 4*a*), which must involve strong Bragg reflections, are: (*a*) the degree of orthogonality of the intersection; (*b*) the multiplicity of rings making the intersection; (*c*) complete resolution of all intersections over the whole of the temperature range, avoiding coalescence such as in Fig. 4(*b*); (*d*) high mobility of the intersection over the temperature range of the experiment (high-angle conics are the most mobile, but there is a trade-off between this and the diffuseness of the ring, see Fig. 5); and (*e*) the occurrence of as many suitable intersections as possible

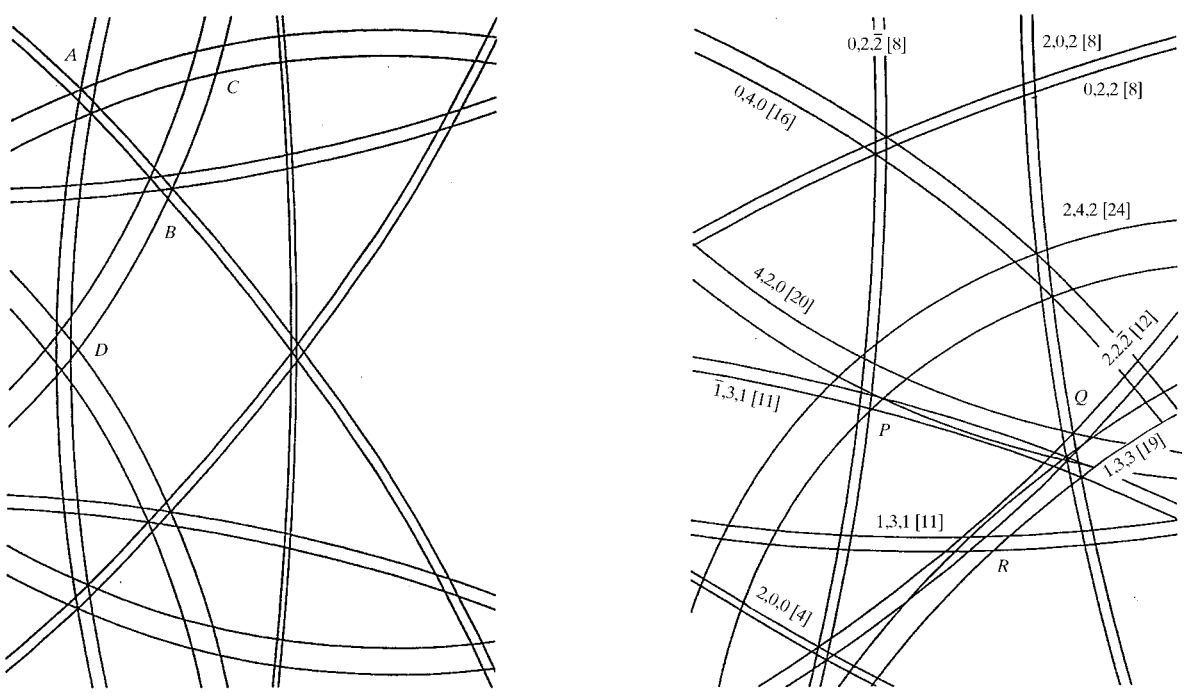

Fig. 4. Computer-generated divergent-beam patterns (*a*) with and (*b*) without mirror symmetry for LiF using extreme values of the cell parameter likely to be encountered in these experiments ($a = 4.00$ and $a = 4.05$ Å) for windows selected for data collection. Note that the value in square brackets, $[\sum(h^2 + k^2 + l^2)]$, on the labelled conics in (*b*) increases with the increase in the thermal spread. The way in which the mutual separation of the various intersections changes with temperature can be seen, and hence intersections that are likely to result in temperature-sensitive line ratios can be selected. In (*a*), the positions of the triple points *A* and *B* will be better defined than the non-orthogonal intersection *C*, and *D* will be complicated by an accidental coincidence, while in (*b*) intersections *P*, *Q* and *R* will be difficult to interpret.

together in the small window (semi-apical angle ~20°) available in the divergent-beam camera.

In this study, computer-generated divergent-beam patterns were initially used to determine the most suitable area of the divergent-beam pattern from which to take experimental divergent-beam photographs over the whole temperature range. As the divergent-beam patterns are usually too complicated to be indexed by inspection, this is performed by comparison with an equivalent computer-generated plot. The experimental divergent-beam data were subsequently compared with the data from computer-generated patterns to determine the values of the cell parameters across the temperature range. In order to optimize the collection of the most sensitive intersections, suitable reflections need to be identified and to establish the crystal orientation to be used. To this end the following strategy was adopted:

The strengths of the reflections were calculated using a structure-factor least-squares program and ~10 of the strongest reflections used as a starting set. The reduced number of reflections is to prevent overcrowding of the stereogram. *A suitable X-ray target* is then selected after inspection of possible θ_{hkl} values for the strong reflections calculated for elements in the range $Z = 16$ to $Z = 40$. The lower limit is determined by the absorption of the Be window and the upper limit by the available kV. In this case, Cu happens to be very suitable.

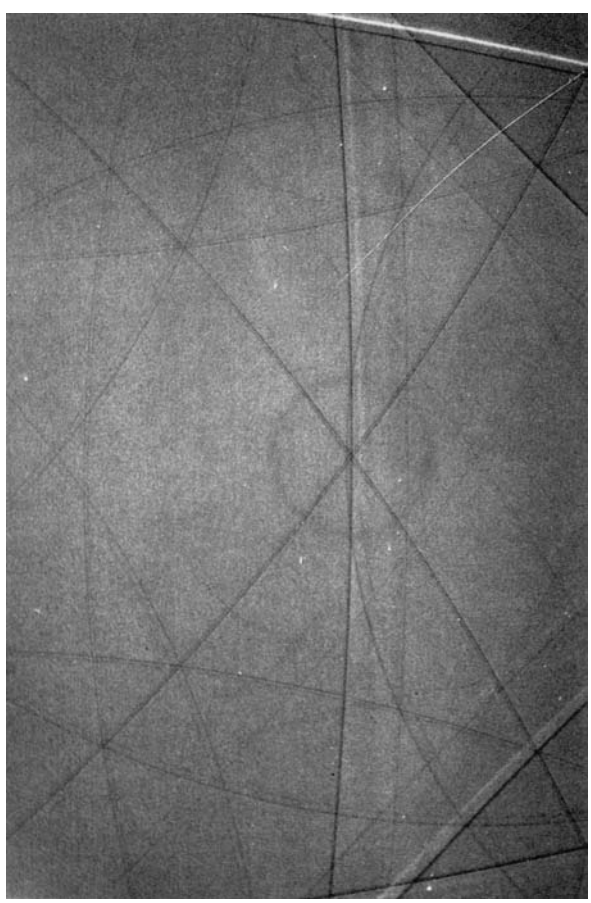

Fig. 5. A divergent-beam photograph of ^{6}LiF for comparison with Fig. 4(*a*). As this is a print, the depletion conics are the dark lines. α_1, α_2 and β conics appear, but only α_1 conics have been considered.

The range of ceIl parameters likely to be involved in a particular thermal-expansion sequence can be roughly estimated from the fact that near absolute zero the r.m.s. amplitude of thermal vibration $u \simeq 0.1$ Å, whereas near the melting point $u \simeq 20\%$ of the bond length. In the case of LiF, the required range is from 4.00 to 4.05 Å over the temperature range 0–380 K.

A pair of computed graph plots (Figs. 3*a*, *b*) of the whole of the divergent-beam pattern for either end of the cell-parameter range was inspected for *windows involving 'good'* intersections. It can be seen that the intersections that appear 'good' at one temperature may not be good at all temperatures.

The pattern within the selected window is plotted as a superimposed 'nest' across the expected range of the cell parameter at $0.1\times$ range intervals, to *check that the selected intersections behave properly*.

A single-crystal camera is then used to set the crystal with the chosen window axis for the divergent-beam pattern positioned along the window axis in the Stereoscan, and a photograph (Fig. 5) obtained.

4. The scanning-electron-microscope (SEM) experimental system

The advantages of using the scanning-electron-microscope environment for the experiments are that (*a*) there is no instrumental broadening, (*b*) the selection of X-ray target materials is not restricted to those commercially available in sealed tubes and (*c*) at liquid-helium temperatures the conics become stronger as the θ values increase, which improves the accuracy to which cell parameters and hence cell volumes can be determined with respect to variations in the isotopic content. The beam in a conventional X-ray tube has a focus ~mm^2 produced by a current of ~mA, which is not suitable for accurate divergent-beam measurements. The X-ray beam in a SEM is generated from a current ~μA with a focus of ~μm^2, which thus has approximately the same current loading as in a conventional tube, so that exposure times are 3–5 min using normal X-ray film. Because the focal spot size is only ~5μm^2, the absorption conics are extremely sharp, regardless of the thickness of the crystal, and for very perfect crystals are too narrow to be recorded. It is therefore necessary to have some degree of imperfection to obtain conics broad enough to be visible, and the crystal must be of a suitable thickness to produce conics of adequate contrast relative to the transmitted white radiation, which provides the overall background.

The low temperatures are achieved by means of a continuous-flow liquid-He cold finger, designed and made for us by Oxford Instruments Ltd, incorporating a

large flange making a vacuum joint with an *O*-ring seal so that it can be mounted in any suitable vacuum jacket. In this application, it is substituting for the liquid-N_2 cold finger on a hot/cold stage in the Cambridge Stereoscan S4 so that divergent-beam pictures can be taken down to liquid-He temperatures. The temperature control and measurement systems were also supplied by Oxford Instruments Ltd. The crystal was attached to the cold finger by means of a thermally conducting copper braid, but the temperature measured was that of the cold finger itself, and may thus not have been the actual temperature of the crystal.

The Kossel camera supplied by David Dingley (Physics Department, Bristol University, England) consists of an insert fitted permanently in one of the Stereoscan stage ports, allowing X-rays generated by the electron beam to exit the SEM through the 5×5 cm Be window, whose distance from the specimen can be varied by means of spacers, and is currently about 10 cm. We have modified the camera to provide two parallel film positions and to carry a filter bar and a digital radiation monitor that can be calibrated to act as an exposure meter. Exposure times are currently 1–5 min using a reasonably fine grain film. The area of the divergent-beam pattern that can be recorded on the film in the Kossel camera is limited by the window area to a cone with a semi-apical angle of $\sim 20^\circ$. A general view of the Kossel camera and low-temperature stage is shown in Fig. 6.

5. Experimental procedure

Having determined the most suitable orientation, the crystal was set using a single-crystal camera and then transferred to the SEM vacuum chamber where the crystal mounting was strapped to the liquid-helium cold finger by the thermally conducting copper braid. Because of uncertainty concerning the actual crystal temperature, data runs were made with the temperature increasing and with it decreasing, allowing time for the crystal temperature to equilibrate at each stage. Significant variations were not observed, but the fact that all the fitted lines (see below) showed a slight upturn at the lowest temperatures indicates that the lowest temperature indicated was not in fact reached.

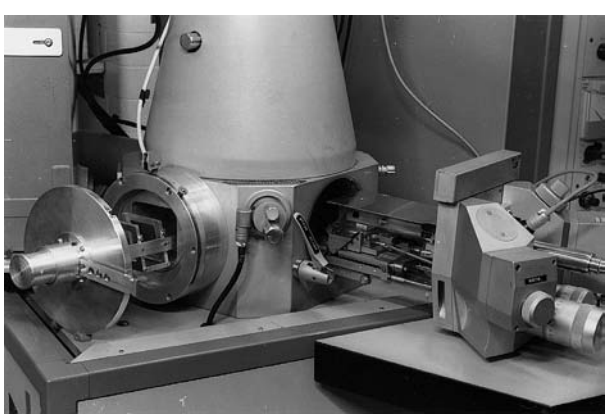

Fig. 6. The Stereoscan with the Kossel camera and cold-stage assembly. The Kossel camera is open to show the two parallel film positions.

5.1. *Generation of divergent X-ray beam*

For optimum conic generation, it is necessary for the divergent-beam source to be as close as possible to the crystal. In practice, this is achieved by dusting the crystal with powder of the element concerned, in this case copper, and then focusing the electron beam on a particle in a suitable position to generate X-radiation producing a divergent-beam pattern on the film. This is performed using the normal SEM electron image screen in the usual way. Trial patterns are then taken to check that the correct orientation has been chosen or to adjust it if necessary and to establish the exposure time required. This will depend on the type of film used, the thickness of the crystal and its degree of mosaicity. For these experiments, using normal X-ray film (Industrial G), the exposure times were about 3–5 min.

5.2. *Temperatures at which films were obtained*

With an allowance of 5 min for the temperature to stabilize at each stage, 15–20 films, the sequence used, were obtained in about 3 h for an increasing or decreasing temperature sequence. Some tests that were made involving films taken at similar or interpolated temperature readings during increasing or decreasing temperature cycles suggested that equilibrium values were being reached.

6. Film measurement and data processing

A primary consideration was to assess the accuracy to be expected from such experiments, since in principle the technique offers a very attractive way of determining thermal-expansion coefficients. Accordingly, for the three members of the LiF isotopic suite investigated, three different window orientations were chosen: (*a*) for ^{6}LiF, an orientation including a mirror plane was selected; (*b*) for 50% ^{6}LiF, an orientation near to this mirror plane was chosen; and (*c*) for ^{7}LiF, an asymmetrical orientation was used. In fact, the ^{7}LiF crystal did not yield useful information because it cracked during the experiment, but such data as were obtained showed that conic intersections complicated by accidental coalescence (Fig. 4*b*) of neighbouring conics were difficult to resolve, although this was the technique favoured by Lonsdale (1947) when investigating cell-parameter variations among individual diamond crystals and is obviously one option that can be considered in such experiments.

It might be supposed that photometer measurements would provide a simple solution, but tests with a drum

scanner and the Isodensitracer, a very suitable instrument when X, Y coordinates are required, had shown that the relatively fast X-ray film used here was too grainy to permit adequate measurements to be obtained for intersection positions in the very low contrast divergent-beam patterns. Transfer of the patterns to an image-analysis system (which would allow the contrast to be intensified) *via* a TV camera was likely to involve some distortion. As originally found by Lonsdale (1947), the human eye is very sensitive to the small density changes involved (~3%), and it was decided that direct measurement using a 5 × 5 cm micrometer stage and a low-power objective would be the most satisfactory procedure to use.

The X, Y coordinates of the intersections on the film were therefore measured using a binocular microscope with a stage controlled by digital micrometers having a resolution of 0.01 mm. Each film was measured three times to provide a standard deviation for the data. For any given line, length variations were plotted as a function of temperature, and a line fitted by a third-order polynomial was superposed upon the measured data. Such variations are expected to be a smooth function of temperature, since no phase change is involved. This procedure allowed lines for which individual lengths at some temperatures lay, for whatever reason, outside one standard deviation from the fitted line, to be rejected (Fig. 7*b*), while lines which provided a good fit to the appropriate polynomial (Fig. 7*a*) were retained for use in ratios.

Ratios of the line lengths for known values of the cell parameters were calculated as part of the graphical simulations. From a combination of these two sets of ratios, the relationship of the cell parameters to temperature can be evaluated.

7. Computational procedure used

The number of available line ratios increases rapidly as the number of intersections, N, involved increases: N intersections $\rightarrow$ $(N^2 - N)/2$ lines $\rightarrow$ $\{[(N^2 - N)/2]2 - (N^2 - N)/2\}/2$ line ratios All line lengths and line ratios for the measured intersections were computed, but *the crucial problem is how to evaluate them.* One possible procedure would be to calculate estimated standard deviation (e.s.d.) values for all the ratios and use them to define the acceptance criteria but, in practice, it was found that because **a**, and therefore the line lengths, varies smoothly with temperature, the most efficient way of deciding to accept/reject lines was *via* an interactive visual presentation of a polynomial fitted to the line length *versus* temperature graphs (Figs. 7*a*, *b*). When a large number of lines is available, it is not cost-effective to investigate the reasons why some values are inaccurate, but it would be possible to do so if required.

The coefficients of the fitted polynomials were then used to determine the 'smoothed' experimental line length (LE) between two intersections at 10 K intervals.

$$\mathrm{LE}_{i1,i2}(T) = a_0 + a_1 T + a_2 T^2 + a_3 T^3.$$

A similar procedure was applied to the calculated data to provide a set of line lengths (LC) at 0.005 Å intervals across the predicted cell parameter range.

$$\mathrm{LC}_{i1,i2}(\mathrm{CP}) = b_0 + b_1 \mathrm{CP} + b_2 \mathrm{CP}^2 + b_3 \mathrm{CP}^3.$$

The ratio of a pair of calculated lines across the cell parameter range can be

$$\mathrm{RC} = \mathrm{LC}_{i1,i2}/\mathrm{LC}_{i3,i4}$$

fitted to a third polynomial:

$$\mathrm{CP}_{\mathrm{calc}} = c_0 + c_1 \mathrm{RC} + c_2 \mathrm{RC}^2 + c_3 \mathrm{RC}^3$$

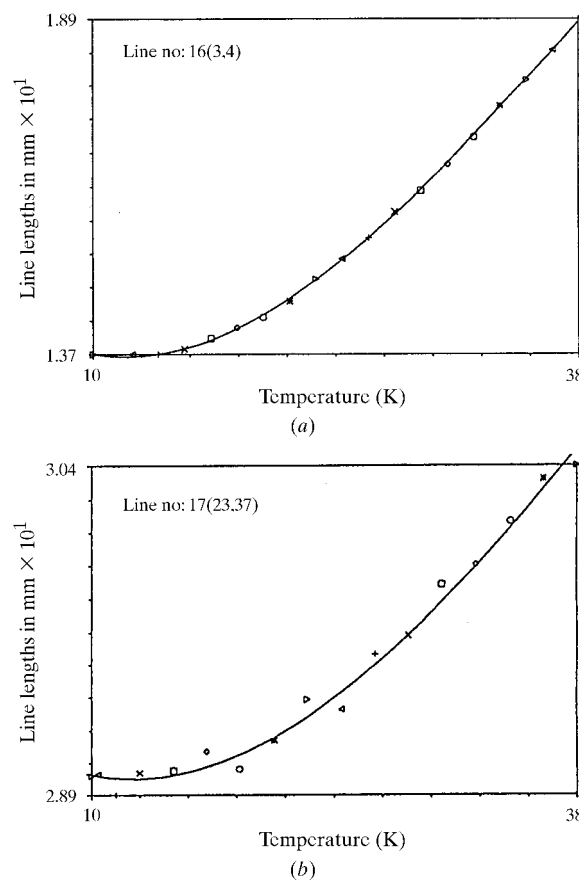

Fig. 7. Plots, *versus* temperature, of the values of individual line lengths obtained for a particular pair of intersections on each film in the sequence indicating which varied smoothly, *i.e.* both measurement accuracy and temperature determination were satisfactory (*a*) (to be retained), and which gave, for whatever reason, large deviations from a fitted polynomial (*b*) (to be rejected). The small deviations of good lines were generally all positive or all negative for a particular film, suggesting that the measured temperature was slightly in error for that film.

and using the coefficients $(c_0, \ldots, c_3)$ in conjunction with the ratio of the experimental lines

$$\mathrm{RE} = \mathrm{LE}_{i1,i2}/\mathrm{LE}_{i3,i4},$$

the cell parameter (CP) can be determined from

$$\mathrm{CP}_{\mathrm{exp}} = c_0 + c_1\mathrm{RE} + c_2\mathrm{RE}^2 + c_3\mathrm{RE}^3,$$

giving a value of $\mathrm{CP}_{\mathrm{exp}}$ at intervals of 10 K across the temperature range.

8. Assessment of errors involved in the measurements

The largest source of error that cannot be accurately assessed in these experiments is the specimen temperature, because the crystal mount is connected to the thermocouple by a copper braid, so that the value of the temperature recorded is not necessarily correct. Hence, the deviation of the measured line lengths from a smooth temperature dependence will be due to a combination of position-sensitive errors and temperature errors. The effect of these errors can be illustrated in two ways:

(I) The range of cell-parameter values recorded for any given film (*i.e.* at constant temperature) will be due to *position-sensitive errors.* Fig. 8 shows the spread of values for 28 ratios from 5 particular films, and it is obvious that systematic differences of individual ratios do occur, as can be seen by examining the plots for all the smooth lines fitted to the line length *versus* temperature graphs such as Fig. 7(*b*), where some line lengths have a tendency to a positive deviation from the line and others a negative one. Cell parameters for acceptable ratios have a spread of $\sim\pm0.001$ Å, and the mean value has an e.s.d. of ~0.0001 Å for a single film.

(II) Systematic deviations from the smoothed lines could also be due to errors in the temperature measurement. Inspection of deviations for good lines shows that they are in the same direction for all lines for a particular temperature, *i.e.* for an individual film, and this suggests that the assumed temperature is incorrect. However, such errors are smaller than position-sensitive errors for a sequence of films obtained in a single experimental run. The effect of cell-parameter variations, owing to likely errors in temperature measurement, on the line lengths can be illustrated by calculating the line length to be expected at a given temperature for the actual cell parameter obtained, *rounded to the nearest 0.0005 Å so that deviations should not exceed 0.00025 Å.* Such errors, which correspond to temperature errors of ~2.5 K at room temperature, are just detectable and can be compared with measured data for the same lines. Therefore, it is possible for ratios from a few good line lengths to define precise cell-parameter variations with temperature, but these might be subject to a slight systematic error. It seems unlikely that temperature rises greater than this would be generated by currents of a few microamps in 3–5 min, as opposed to currents of milliamps from conventional X-ray tubes. The thermal-expansion coefficient at room temperature, confirmed as 0.00014 Å/K (Thewlis, 1955), means that errors of ~3.0 K in the temperature measurement would be sufficient to eliminate the difference (0.0006 Å)

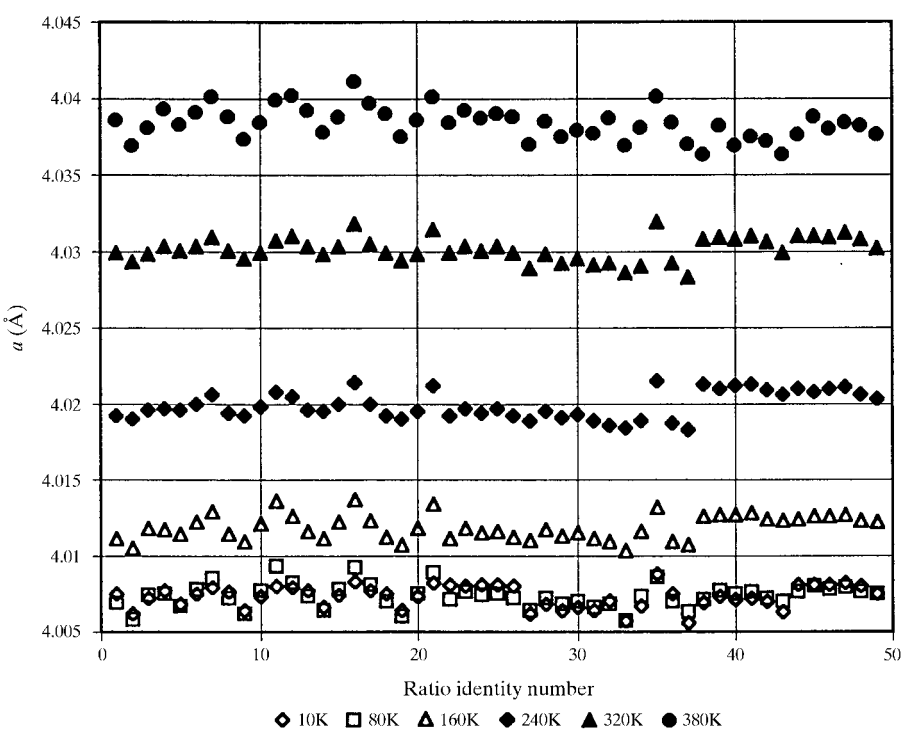

Fig. 8. Variations of cell parameters obtained from individual ratios for six films selected from the $^6LiF_{90.4\%}$ sequence. Average values and standard deviations were obtained for such sequences.

between the lattice parameters of 90.4% ^{6}LiF and 50% ^{6}LiF. Care was taken therefore to take photographs at the same recorded temperatures for both crystals to within 0.5 K and often to within 0.1 K, and to allow time for the system to equilibrate at each new temperature setting. Temperature measurement below 30 K is likely to be much less accurate, and in spite of good heat shielding is always likely to give a value lower than the actual specimen temperature. On the other hand, the fact that $\delta a/\delta T \rightarrow 0$ as $T \rightarrow 0$ means that changes found in this region will be difficult to detect, and films taken at nominal temperatures of 14 and 19 K confirm that position-sensitive errors are more important than temperature errors.

Fig. 7(*a*) also shows why the cell parameters obtained from the smoothed data appear to increase slightly as $T \rightarrow 0$, because even when the polynomial is fitted to a group of identical **a** values in the range $T = 0 \rightarrow 50$ K, it shows an inflection near $T = 0$ K. Attempts to fit functions constrained to produce $\delta\mathbf{a}/\delta T = 0$ at $T = 0$, such as a parabola, did not provide a more satisfactory fit over the whole temperature range. The existence of this apparent inflexion contributed to the difficulty of distinguishing between parameter values at 80 and 10 K in Fig. 8.

9. Results

Graphs for cell parameter *versus* temperature were drawn for 90.4% ^{6}LiF and 50.1% ^{6}LiF (Fig. 9), from which the room-temperature cell parameters were compared with those of Thewlis (l955). As can be seen from the graph, there is a significant difference in the cell parameters at liquid-He temperatures for the two isotopically distinct compounds. Reading from the smoothed graphs, our cell parameters at 298 K become $^6\mathrm{Li}_{90.4\%} = 4.0272\ (2)$ Å and $^6\mathrm{Li}_{50.2\%} = 4.0266\ (2)$ Å. An assumption that the stated isotopic compositions

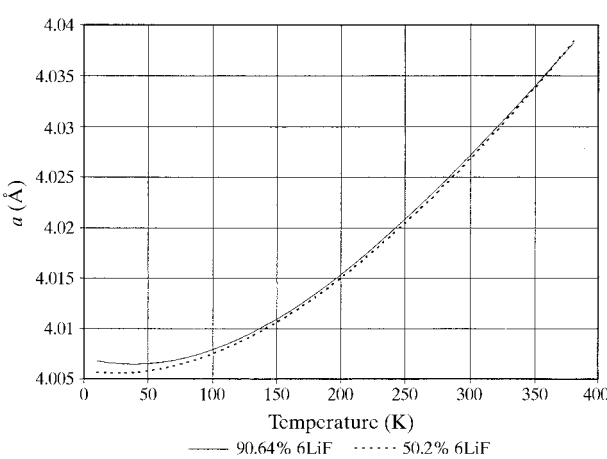

Fig. 9. Comparison of the cell dimensions *versus* temperature for $^6\mathrm{LiF}_{90.4\%}$ and $^6\mathrm{LiF}_{50.2\%}$ obtained from the two film sequences. Thermal-expansion coefficients can be calculated from these data.

are correct, linear extrapolation to end-member cell parameters gives $a_{100\%} = 4.0273\ (2)$ and $a_{0\%} = 4.0259\ (2)$ Å, as compared with $a_{100\%} = 4.0271\ (1)$ Å and $a_{0\%} = 4.0263\ (1)$ Å reported by Thewlis (1955). Unfortunately, the $^6\mathrm{Li}_{\sim 0\%}$ specimen cracked during the experiment, and no useful results were obtained for it. A measurement of natural-abundance LiF at 98 K, which approximates to $^6\mathrm{Li}_{7.5\%}$, *i.e.* close to $^6\mathrm{Li}_{0\%}$, was given by Straumanis (1949) as $a = 4.02620\,(5)$ Å, and it was stated that this value had been corrected for refraction. With the assuption that the required correction to be subtracted from the measured value can be evaluated for cubic crystals from the equation (Lipson & Wilson, 1941) $d(l - n) = 4.47 \times 10^{-6}(\lambda/a)^2 \sum Z$, where $\sum Z$ is the sum of the atomic numbers of all the atoms in the unit cell, the correction for Cu $K\alpha$ radiation would be 31.4×10^{-6}, making the measured value 4.02623 (5) Å. Thewlis did not make a refraction correction, but confirmed the value with measurements of Johnson Matthey 'specpure' LiF. Our extrapolated value for natural LiF would be 4.0260 (2) Å, so, although in principle a refraction correction should be made, it can be seen that the estimated experimental errors are too large to justify such a correction.

10. Conclusions

There is no doubt that such experiments can provide a rapid method of obtaining cell-parameter measurements as a function of temperature. With the increasing power of computers, procedures for considering film shrinkage, crystal perfection and the geometrical quality of intersections could be incorporated in the analysis programs and, with the addition of a camera with a Be window on a SEM port, this method is likely to provide one of the simplest and most cost-effective ways of obtaining thermal-expansion data for crystals of any symmetry.

These experiments would not have been possible without the assistance of Mr P. A. Woods, who was responsible for many aspects of the design and construction of the SEM system, and for the actual data collection on which these results are based. We are grateful to the Royal Society for permission to reproduce Fig. l of Lonsdale (1947).

References

Berman, R. (1976). *Thermal Conduction in Solids.* Oxford: Clarendon Press.
Berman, R. & Brock, J. C. F. (1965) *Proc. R. Soc. London Ser. A*, **289**, 46–80.
Lipson, H. S. & Wilson, A. J. C. (1941). *J. Sci. Instrum.* **18**, 144–148.
Lonsdale, K. (1947). *Philos. Trans. R. Soc. London Ser. A*, **240**, 219–250.
Straumanis, M. E. (1949). *J. Appl. Phys.* **20**, 725–734.
Thewlis, J. (1955). *Acta Cryst.* **8**, 36–38.